affected only a small region of the X chromosome that contains a dosage-sensitive gene[24,25]. □

Methods

Generation of the *Air-T* allele

The targeting vector was constructed from a 9.6-kb *Bgl*II fragment (bp 117,878–127,575; AJ249895). A selection cassette containing *neomycin* and the thymidine kinase gene, each driven by a PGK promoter flanked by loxP sites plus a 1.2-kb fragment from the rabbit β-globin gene (bp 31,392–32,590; M18818) containing part of exon 2, complete intron 3 and complete exon 3 with the polyadenylation signal in the correct orientation for the *Air* promoter, was inserted at the *Bam*HI site in this fragment. The selection cassette was deleted by electroporation of a plasmid encoding Cre recombinase[26] and transient puromycin selection. We generated chimaeric mice by injecting paternally targeted *Air-T* embryonic stem (ES) cells into C57/Bl6 blastocysts[27]. Mice carrying the *Air-T* allele were maintained on an FVB/N background.

Methylation and expression analyses

Digestion of methyl-sensitive enzymes was monitored by hybridization to mitochondrial DNA. We carried out RPA using an RPAIII kit (Ambion). Signals were quantified with a Phosphorimager (Fujix). For RT-PCR, 5 μg heart RNA was reverse transcribed with Superscript (Gibco) using the linker-poly(dT) primer RT, 5′-CTGGGAAACAGCTATGACCATGATCGATTTTTTTTTTTTTTTTN-3′, and amplified with PX6R, 5′-GAAGCACAGCACCGCCAGTTAC-3′, for 30 cycles (94 °C, 30 s; 59 °C, 30 s; 72 °C, 120 s).

Probes for DNA analyses

We used the following probes: probe A, a 325-bp PCR fragment (bp 102,813–103,137; AJ249895); probe C, a 0.9-kb *Eco*RI/*Hin*CII fragment from EST AA592338 (ref. 6) collinear with genomic DNA; probe D, (bp 121,834–122,862; AJ249895); and probe E (bp 124,992–126,086; AJ249895).

Probes for RNA analyses

Probe B, described as probe GFPAIR[14], is 322 bp and protects 185 bp of *Air* RNA at the *Igf2r* promoter. Probes C and D are the same as the DNA analyses probes. Probe F is 174 bp and protects 47 bp (bp 126,181–126,227; AJ249895) immediately downstream from the principal *Air* transcription start site[6]. Probe G (bp 126,086–126,293; AJ249895), described as probe MlMs1 (refs 6,14), detects unspliced (207, 171 and 148 bp) *Air* RNA fragments. This relatively large probe did not produce a clear signal for the spliced *Air-T* RNA (predicted fragments of 112, 76 and 53 bp), which should have been recognized (see probe K below). Probe H, described as probe RPA1 (ref. 6), protects 221 bp of *Air* RNA (bp 85,250–85,029; AJ249895). Probe I, described as probe MS1B8 (ref. 6) protects 196 bp. Probe J is 173 bp and protects 155 bp of *Air* RNA (bp 123,233-123,387; AJ249895). Probe K is 364 bp, contains the RT-PCR fragment made with probes RT and PX6R (Supplementary Information) and protects 287 bp of spliced and 240 and 47 bp of unspliced polyadenylated RNA. Probe L spans 558 bp (bp 32,032–32,590; M18818) of the β-globin gene (including the polyadenylation signal) and protects 173 bp of polyadenylated RNA (bp 32,032–32,204; M18818). Probe L extends 385 bp downstream from the polyadenylation signal and the absence of protected fragments longer than 173 bp indicates use of the polyadenylation signal. The *Aprt* template is a 252-bp *Xho*I/*Xba*I fragment (bp 2,165–2,417; M11310) and protects *Aprt* exon 3 (134 bp). For RNA blots, we used the following probes: for *Igf2r*, complementary DNA exons 3–6; for *Slc22a2*, bp 989–1,605 (AJ006036); for *Slc22a3* bp 1–2,766 (AF078750); for *Gapd*, complete cDNA.

Received 27 September; accepted 4 December 2001.

1. Reik, W. & Walter, J. Genomic imprinting: parental influence on the genome. *Nature Rev. Genet.* **2,** 21–32 (2001).
2. Sleutels, F. & Barlow, D. P. in *Homology Effects* (eds Wu, C.-t. & Dunlap, C.) (Academic, San Diego, in the press).
3. Wutz, A. *et al.* Imprinted expression of the *Igf2r* gene depends on an intronic CpG island. *Nature* **389,** 745–749 (1997).
4. Wutz, A. *et al.* Non-imprinted *Igf2r* expression decreases growth and rescues the Tme mutation in mice. *Development* **128,** 1881–1887 (2001).
5. Zwart, R., Sleutels, F., Wutz, A., Schinkel, A. H. & Barlow, D. P. Bidirectional action of the *Igf2r* imprint control element on upstream and downstream imprinted genes. *Genes Dev.* **15,** 2361–2366 (2001).
6. Lyle, R. *et al.* The imprinted antisense RNA at the *Igf2r* locus overlaps but does not imprint Mas1. *Nature Genet.* **25,** 19–21 (2000).
7. Beechey, C. V., Cattanach, B. M. & Selley, R. L. Mouse Imprinting Data and References. *MRC Mammalian Genetics Unit* [online] ⟨http://www.mgu.har.mrc.ac.uk/imprinting/imprinting.html⟩ (2000).
8. Schmidt, J. V., Levorse, J. M. & Tilghman, S. M. Enhancer competition between H19 and *Igf2* does not mediate their imprinting. *Proc. Natl Acad. Sci. USA* **96,** 9733–9738 (1999).
9. Hark, A. T. *et al.* CTCF mediates methylation-sensitive enhancer-blocking activity at the H19/*Igf2* locus. *Nature* **405,** 486–489 (2000).
10. Constancia, M. *et al.* Deletion of a silencer element in *Igf2* results in loss of imprinting independent of H19. *Nature Genet.* **26,** 203–206 (2000).
11. Bell, A. C. & Felsenfeld, G. Methylation of a CTCF-dependent boundary controls imprinted expression of the *Igf2* gene. *Nature* **405,** 482–485 (2000).
12. Reik, W. & Murrell, A. Genomic imprinting. Silence across the border. *Nature* **405,** 408–409 (2000).
13. Wang, Z. Q., Fun, M. R., Barlow, D. P. & Wagner, E. F. Regulation of embryonic growth and lysosomal targeting by the imprinted *Igf2/Mpr* gene. *Nature* **372,** 464–467 (1994).
14. Sleutels, F. & Barlow, D. P. Investigation of elements sufficient to imprint the mouse Air promoter. *Mol. Cell. Biol.* **21,** 5008–5017. (2001).
15. Wroe, S. F. *et al.* An imprinted transcript, antisense to Nesp, adds complexity to the cluster of imprinted genes at the mouse Gnas locus. *Proc. Natl Acad. Sci. USA* **97,** 3342–3346 (2000).
16. Lee, Y. J. *et al.* Mit1/Lb9 and Copg2, new members of mouse imprinted genes closely linked to Peg1/$Mest_1$. *FEBS Lett.* **472,** 230–234 (2000).
17. Rougeulle, C., Cardoso, C., Fontes, M., Colleaux, L. & Lalande, M. An imprinted antisense RNA overlaps UBE3A and a second maternally expressed transcript. *Nature Genet.* **19,** 15–16 (1998).
18. Smilinich, N. J. *et al.* A maternally methylated CpG island in KvLQT1 is associated with an antisense paternal transcript and loss of imprinting in Beckwith-Wiedemann syndrome. *Proc. Natl Acad. Sci. USA* **96,** 8064–8069 (1999).
19. Avner, P. & Heard, E. X-chromosome inactivation: counting, choice and initiation. *Nature Rev. Genet.* **2,** 59–67 (2001).
20. Clemson, C. M., McNeil, J. A., Willard, H. F. & Lawrence, J. B. XIST RNA paints the inactive X chromosome at interphase: evidence for a novel RNA involved in nuclear/chromosome structure. *J. Cell Biol.* **132,** 259–275 (1996).
21. Lee, J. T., Strauss, W. M., Dausman, J. A. & Jaenisch, R. A 450 kb transgene displays properties of the mammalian X-inactivation center. *Cell* **86,** 83–94 (1996).
22. Sheardown, S. A. *et al.* Stabilization of Xist RNA mediates initiation of X chromosome inactivation. *Cell* **91,** 99–107 (1997).
23. Wutz, A. & Jaenisch, R. A shift from reversible to irreversible X inactivation is triggered during ES cell differentiation. *Mol. Cell* **5,** 695–705 (2000).
24. Lyon, M. F. Imprinting and X-chromosome inactivation. *Results Probl. Cell Differ.* **25,** 73–90 (1999).
25. Graves, J. A. Mammals that break the rules: genetics of marsupials and monotremes. *Annu. Rev. Genet.* **30,** 233–260 (1996).
26. O'Gorman, S., Dagenais, N. A., Qian, M. & Marchuk, Y. Protamine-Cre recombinase transgenes efficiently recombine target sequences in the male germ line of mice, but not in embryonic stem cells. *Proc. Natl Acad. Sci. USA* **94,** 14602–14607 (1997).
27. Hogan, B. L. M., Beddington, R. S. P., Costantini, F. & Lacy, E. *Manipulating the Mouse Embryo* (Cold Spring Harbor Laboratory Press, Cold Spring Harbor, 1994).

Supplementary Information accompanies the paper on *Nature*'s website (http://www.nature.com).

Acknowledgements

We thank K. van Veen, K. van het Wout, P. Krimpenfort for help in generating mice; S. Greven, T. Maidment and N. Bosnie for care of the mice; A. Berns, H. te Riele, M. van Lohuizen, R. Beijersbergen, P. Borst and A. Frischauf for comments; and A. Berns for help and encouragement. This research was supported by the Dutch Cancer Society (KWF).

Correspondence and requests for materials should be addressed to D.P.B. (e-mail: dbarlow@imb.oeaw.ac.at).

Structural basis for antagonist-mediated recruitment of nuclear co-repressors by PPARα

H. Eric Xu, Thomas B. Stanley, Valerie G. Montana, Millard H. Lambert, Barry G. Shearer, Jeffery E. Cobb, David D. McKee, Cristin M. Galardi, Kelli D. Plunket, Robert T. Nolte, Derek J. Parks, John T. Moore, Steven A. Kliewer, Timothy M. Willson & Julie B. Stimmel

Nuclear Receptor Discovery Research, GlaxoSmithKline, Research Triangle Park, North Carolina 27709, USA

Repression of gene transcription by nuclear receptors is mediated by interactions with co-repressor proteins such as SMRT and N-CoR[1,2], which in turn recruit histone deacetylases to the chromatin[3–5]. Aberrant interactions between nuclear receptors and co-repressors contribute towards acute promyelocytic leukaemia and thyroid hormone resistance syndrome[6–8]. The binding of co-repressors to nuclear receptors occurs in the unliganded state, and can be stabilized by antagonists[9]. Here we report the crystal structure of a ternary complex containing the peroxisome proliferator-activated receptor-α ligand-binding domain bound to the antagonist GW6471 and a SMRT co-repressor motif. In this structure, the co-repressor motif adopts a three-turn α-helix that prevents the carboxy-terminal activation helix (AF-2) of the receptor from assuming the active conformation. Binding of

the co-repressor motif is further reinforced by the antagonist, which blocks the AF-2 helix from adopting the active position. Biochemical analyses and structure-based mutagenesis indicate that this mode of co-repressor binding is highly conserved across nuclear receptors.

The peroxisome proliferator-activated receptor-α (PPARα) regulates hepatic fatty acid metabolism and mediates the effects of fibrate lipid-lowering drugs[10]. We recently described the L-tyrosine analogue GW409544 as a potent PPARα agonist[11]. The crystal structure of GW409544 bound to PPARα reveals that the carboxylic acid group of GW409544 makes a direct hydrogen bond with Y464 on the C-terminal AF-2 helix, and this interaction stabilizes the receptor in the active confirmation[11]. On the basis of these observations, we designed a PPARα antagonist by substituting an ethyl amide group for the acid group of GW409544 to disrupt the hydrogen bond with Y464 (Fig. 1a). The resulting compound, GW6471, is a potent PPARα antagonist. In a cell-based reporter assay, GW6471 completely inhibited GW409544-induced activation of PPARα with a median inhibitory concentration (IC_{50}) of 0.24 μM (Fig. 1b).

The transcriptional activity of nuclear receptors is a function of their interactions with coactivators such as SRC-1 (steroid receptor coactivator-1)[12] or CBP (CREB-binding protein), or co-repressors such as N-CoR (nuclear co-repressor) and SMRT (silencing mediator for retinoid and thyroid hormone receptors). Coactivators contain an LXXLL motif that forms two turns of α-helix and binds into a hydrophobic cleft on the surface of the receptor. In the PPARα/GW409544/SRC-1 structure, the SRC-1 coactivator motif is secured by a charge clamp between residues on the AF-2 helix and helix 3, similar to coactivator complexes with oestrogen receptor[13], thyroid receptor[14], retinoid X receptor[15] and PPARγ[15,16]. As nuclear receptor antagonists decrease binding of coactivators and increase binding of co-repressors[9], we examined the effect of GW6471 on the interaction of PPARα with peptides derived from coactivator and co-repressor motifs[17–21]. GW6471 disrupted the interactions between PPARα and coactivator motifs derived from SRC-1 or CBP, but promoted the binding of the co-repressor motifs from SMRT or N-CoR[22] (Fig. 1c). The potency of GW6471 for displacement of coactivators and recruitment of co-repressors matched the IC_{50} value for PPARα antagonism in cell-based assays. The binding affinity of the SMRT or the N-CoR motifs to the PPARα ligand-binding domain (LBD) was enhanced fivefold by GW6471 (Fig. 1d). GW6471 also enhanced the interactions of PPARα with the N-CoR or the SMRT motifs in a mammalian two-hybrid assay (Fig. 1e). These results demonstrate that GW6471 induces a PPARα LBD conformation that interacts efficiently with co-repressors.

Both SMRT and N-CoR contain multiple receptor-interacting motifs[19–21]. To understand the molecular basis of co-repressor recruitment, we determined the crystal structure of a ternary complex containing the PPARα LBD bound to GW6471 and a peptide derived from the C-terminal receptor-interacting motif of SMRT (Figs 2a and 3a). The refined structure contains four PPARα/GW6471/SMRT complexes (see Methods and Table 1), and reveals a clear electron density for the core co-repressor motif and the antagonist GW6471 (Fig. 2b, c). The PPARα LBD contains 13 α-helices and 4 small β-strands that fold into a typical nuclear receptor helical sandwich. The SMRT motif adopts a three-turn α-helix and docks into a hydrophobic groove formed by helices 3, 3′, 4 and 5 (Fig. 2a). Superposition of the agonist- and antagonist-bound PPARα (Fig. 2d) reveals that the co-repressor-binding site partly overlaps with the coactivator-binding site. The additional helical turn in the co-repressor motif extends into the space that is left by the repositioning of the AF-2 helix, and prevents this helix from folding back into its active conformation.

GW6471 adopts a U-shaped configuration and wraps around C276 of helix 3 (Fig. 2c). The modified amide head group of GW6471 adopts a configuration that is no longer able to form a hydrogen bond with Y464 on the AF-2 helix. Instead, this larger head group extends into the space that is normally occupied by the side chain of Y464, and pushes the AF-2 helix out of the agonist-bound position (Fig. 2e). Unlike the previously determined antago-

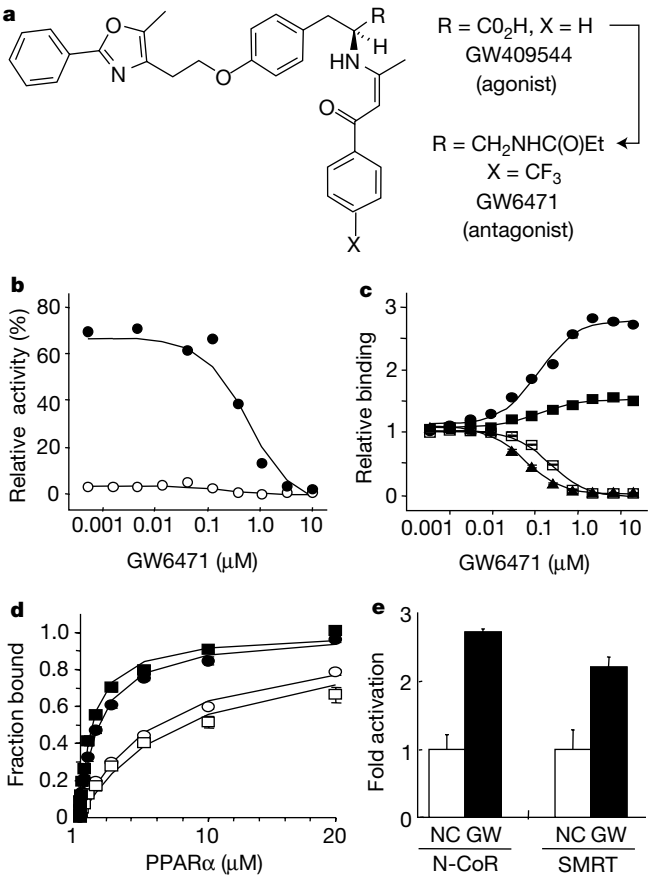

Figure 1 GW6471 recruits co-repressors to PPARα. **a**, Chemical structures of GW409544 and GW6471. **b**, Effect of GW6471 on activation of PPARα in the presence (filled circles) or absence (open circles) of 10 nM GW409544. **c**, Fluorescence energy transfer assays for the effect of GW6471 on peptide binding to PPARα. SMRT, filled circles; N-CoR, filled squares; CBP, filled triangles; SRC-1, open squares. **d**, Binding of SMRT (squares) or N-CoR (circles) motifs to PPARα in the presence (filled) or absence (open) of GW6471, as measured by fluorescence polarization. **e**, Effect of GW6471 on binding of SMRT or N-coR motifs to PPARα in a mammalian two-hybrid assay. NC, no compound; GW, 10 μM GW6471. The results are the average of three experiments, with error bars showing s.d.

Table 1 Statistics of crystallographic data and structures

Crystals	PPARα/SMRT complex	PPARα/SRC-1 complex
Space group	$P2_12_12_1$	$P2_12_12$
Resolution (Å)	30.0–3.0	20.0–1.8
Unique reflections	29,380	30,147
Completeness (%)	99.0	99.4
I/σ	23.3 (2.0)	39.5 (5.2)
R_{sym}* (%)	6.8	4.5
Refinement statistics		
R_{factor}† (%)	25.7	21.9
R_{free} (%)	29.0	26.7
r.m.s.d. bond lengths (Å)	0.008	0.007
r.m.s.d. bond angles (deg)	1.956	1.561
Total non-hydrogen atoms	9,615	2,659

r.m.s.d. is the root-mean-square deviation from ideal geometry.
$R_{sym} = \Sigma|I_{avg} - I_i|/\Sigma I_i$.
$R_{factor} = \Sigma||F_O| - |F_C||/\Sigma|F_O|$, where F_O and F_C are observed and calculated structure factors, R_{free} was calculated from a randomly chosen 10% of reflections excluded from refinement, and R_{factor} was calculated for the remaining 90% of reflections.

nist-bound oestrogen-receptor structures[13], the AF-2 helix does not occupy the coactivator-binding groove, but is loosely packed against helix 3 (Fig. 2a, d). The PPARα/SMRT complex reveals that removal of the AF-2 helix from its active position destroys the integrity of the charge clamp but leaves sufficient space to accommodate the additional helical turn of the co-repressor motif.

Although there is overlap in the co-repressor- and coactivator-binding modes, there are numerous differences in their binding interfaces. First, the three helical turns in the co-repressor motif result in a larger interaction interface with PPARα than the two helical turns of the coactivator motif. The SMRT LXXXIXXXL motif covers 736 Å^2 of Connolly surface of PPARα, whereas the SRC-1 LXXLL motif buries only 478 Å^2. The larger co-repressor interaction surface may account for the preferential binding of co-repressor over coactivator to PPARα in the presence of GW6471. Second, the co-repressor helix is anchored to PPARα by three hydrogen bonds between the C-terminal carbonyls and the conserved K292 from helix 3, which also caps the coactivator helix[11]. Compared with the coactivator helix, the co-repressor motif pivots ~15 degrees about its C-terminal end into the void left behind by displacement of the AF-2 helix, bringing the central isoleucine residue (I + 5 in Fig. 3a) 2–3 Å closer to helices 3, 4 and 5 (Fig. 2d, e). The unexpected binding mode of the co-repressor motif provides a structural explanation for the sequence differences between co-repressor and coactivator motifs. The first and the second leucines of the coactivator LXXLL motif are equivalent in the positions of the central isoleucine (+5) and the A + 8 of the co-repressor motif in the superposition of their respective structures. However, the larger leucine side chains at positions +5 and +8 prevent the coactivator LXXLL motif binding tightly to the receptor in the absence of the AF-2 helix, like the co-repressor motif. This is in agreement with previous studies, which found that replacing residue +5 and +8 with leucines in the co-repressor motif results in a non-functional co-repressor[21] The third difference between co-repressor and coactivator binding is that the three-turn helix of the co-repressor motif deviates from a regular α-helix, which allows the residues of L + 1, I + 5 and L + 9 to align on the same face of the helix (Figs 2f and 3b), and to make the core hydrophobic interactions with the receptor. Besides these core interactions, the co-repressor motif makes additional interactions with the receptor through peripheral residues composed by I + 4, A + 8, E + 2 and R + 6, which are oriented at angles of ~90° to either side of the central interface (Fig. 3b). On one side, the side chains of I + 4 and A + 8 are partially exposed and make additional hydrophobic contacts along one ridge of the binding groove. On the opposite side, residues E + 2 and R + 6 form a strong intramolecular H-bond, which positions these residues so as to make a pair of intermolecular hydrogen bonds with K310 and N303 of helix 4. This hydrogen bond network is further strengthened by additional hydrophobic interactions between these two side chains and L302 and V306, which form the ridge on this side of the groove.

We next examined the receptor–co-repressor interface by alanine-scanning mutations of the co-repressor motif (Fig. 3c). Replacement of any of the three core interface residues (L + 1, I + 5 and L + 9) with alanine markedly reduced co-repressor binding. Mutating the peripheral interface residues (E + 2, I + 4, R + 6 and M + 10) also decreased co-repressor binding. The interaction profile of these mutated co-repressor motifs was very

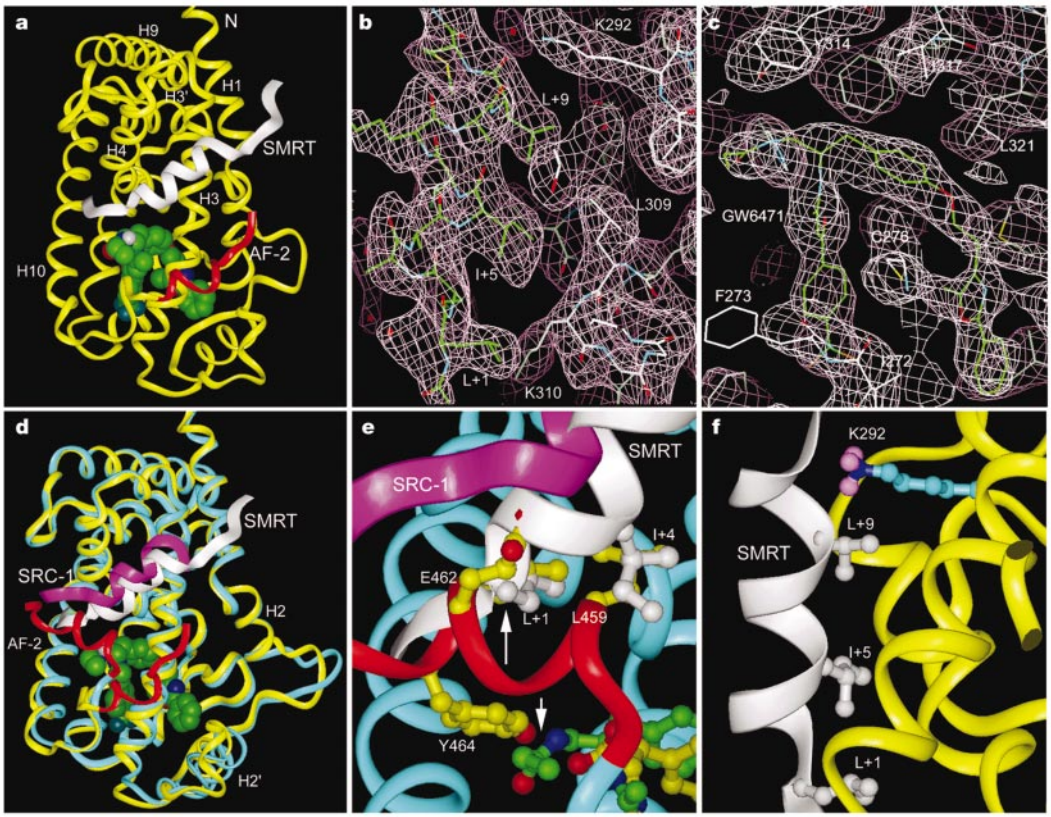

Figure 2 Structure of the PPARα/GW6471/SMRT complex. An overview of the ternary complex. **a**, PPARα LBD, yellow; AF-2 helix, red; SMRT motif, white; GW6471, green spheres. **b**, **c**, Electron density maps of the PPARα–SMRT interface and the antagonist GW6471. The maps are calculated with F_0 coefficiency and contoured at 1σ. The carbon atoms of SMRT and GW6471 are in green. **d**, Overlay of the PPARα/GW6471/SMRT and the PPARα/GW409544/SRC-1 complexes. PPARα LBD, yellow in SMRT complex or blue in SRC-1 complex; SRC-1, purple; SMRT, white. **e**, Superposition of SMRT peptide and GW6471 with the PPARα/GW409544/SRC-1 complex. The short arrow indicates interference between GW6471 and Y464; the long arrow indicates interference between SMRT and the active AF-2 helix. **f**, Interface between PPARα (yellow) and SMRT (white).

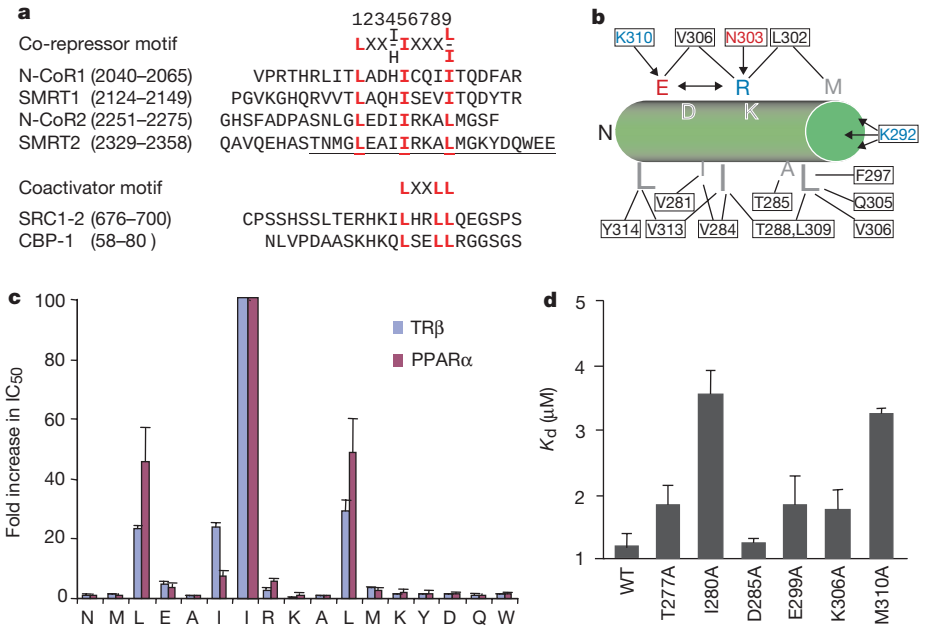

Figure 3 Conservation of co-repressor binding to nuclear receptors. **a**, Co-repressor and coactivator motifs. The underlined sequence was used in crystallography. **b**, Interactions between the SMRT motif (green cylinder) and PPARα (boxed residues). Residue colours: H-bond donors, blue; acceptors, red; hydrophobic contacts, grey (SMRT) and black (PPARα). Arrows indicate hydrogen bonds; lines indicate van der Waals contacts. **c**, Alanine scan of the SMRT2 motif. Binding of peptides to PPARα and TRβ was measured by fluorescence polarization. IC_{50} values for the wild-type SMRT motif are 8.0 ± 3.4 uM and 6.7 ± 2.3 uM for PPARα and TRβ, respectively. **d**, Affinities of mutated TRβ LBDs for the SMRT2 motif as measured by fluorescence polarization. WT, wild type. Error bars are the s.d. of three experimemts.

similar to the one for TRβ(thyroid hormone receptor-β) (Fig. 3c), demonstrating a similar mode of co-repressor binding to these receptors. This idea is further supported by structure-based sequence alignment, which reveals that the residues involved in co-repressor binding are highly conserved across the nuclear receptor family (data not shown). Nine out of the fourteen residues that contact the co-repressor domain in PPARα were previously mutated in TRβ[19–21]. Each of these mutations decreased the interaction between TRβ and the co-repressor motif. We mutated the remaining five contact residues in TRβ and showed that these changes also result in decreases in co-repressor interaction (Fig. 3d). These results suggest that the co-repressor interaction interface observed in PPARα is conserved in other nuclear receptors.

The structure of the PPARα/GW6471/SMRT ternary complex demonstrates that the co-repressor motif adopts an irregular three-turn helix that fits tightly into a receptor groove, which also serves as the coactivator-binding site. Nuclear receptors distinguish co-repressors from coactivators by the length of their helical interaction motifs, which depends on the AF-2 conformation. In the presence of an antagonist, the AF-2 helix is blocked from assuming the active conformation, resulting in a larger pocket that can accommodate the three-turn α-helix of the co-repressor LXXXIXXXL motif. The high degree of conservation of the co-repressor and coactivator interaction interfaces suggests that this is a model that applies to many of the nuclear receptors. □

Methods

Protein preparation

The human PPARα LBD (amino acids 198–468; GenBank accession number S74349) tagged with MKKHHHHHHLVPRG (thrombin cleavage site underlined) was expressed from the T7 promoter of the pRSETA vector (Invitrogen). The wild-type and mutated LBDs of TRβ were also expressed from pRSETA, but were tagged with MKKGHHHHHHG. The proteins were purified as described[23], and the tag was removed from the PPARα LBD by incubation with thrombin (200:1 molar ratio) overnight at 4 °C. The PPARα/GW6471/SMRT complex was prepared by addition of a twofold molar excess of the SMRT2 peptide (sequence referred to in Fig. 3a) and fivefold molar excess of the antagonist, concentrated to ~9.0 mg ml^{-1}, and then aliquoted and stored at −80 °C.

Crystalization and data collection

The PPARα/GW6471/SMRT crystals were grown at room temperature in hanging drops containing 1 μl of the above protein-ligand solutions and 1 μl of well buffer (5.5–9.6% polyethylene glycol (PEG) 35K, 50 mM di-ammonium hydrogen citrate, pH 4.9, 50 mM 1,3 bis-tris-propane (BTP), pH 7.0, 10% MPD). Crystals grew to a size of 100–200 μm within several weeks. Data collections were performed with crystals that were transiently mixed with the well buffer containing an additional 10% 2-methyl-2,4-pentanediol (MPD), and then flash frozen in liquid nitrogen.

The crystals formed in the $P2_12_12_1$ space group, with $a = 103.4$ Å, $b = 112.8$ Å, $c = 123.9$ Å. Each asymmetric unit contained four PPARα LBDs, four SMRT co-repressor peptides and four GW6471 antagonist molecules with a solvent content of 50%. Crystals were screened with a Rigaku R-Axis II detector and data were collected with a MAR CCD (charge-coupled device) detector at 17-ID in the facilities of the Industrial Macromolecular Crystallography Association (IMCA), at the Advanced Photon Source. We processed the observed reflections with the Denzo and Scalepack programs in the HKL2000 package[24].

Structure determination and refinement

The PPARα/GW6471/SMRT structure was determined by molecular replacement methods with the AmoRe program[25] using a 1.8 Å structure of a PPARα/SRC-1 complex as the initial model (Table 1). The best-fit solution generated with AmoRe gave a correlation coefficiency of 36.1% and an *R*-factor of 46.9%. The phases from the molecular replacement were extensively refined with solvent flattening, histogram matching, and fourfold non-crystallographic symmetry (NCS) averaging as implemented in the DM program[26]. The electron density maps were further improved with multiple crystal averaging of three PPARα/SMRT data sets by the DMMULTI program. We applied a negative *b*-factor to the data to enhance the feature of the electron density for the protein side chains[27]. Multiple cycles of manual model building were performed with QUANTA (Molecular Simulations). Structure refinements were proceeded with CNX[28], using the maximum likelihood target and NCS constraints, which was relaxed in the final stages of refinement. The statistics of the structure and data sets are summarized in Table 1.

Functional assays

Cell-based assays for GW6471 as an antagonist were performed in CV-1 cells using the $(UAS)_5$-tk-SPAP reporter and the human PPARα–GAL4 chimaeras as described previously[11]. We carried out transfections using lipofectamine (Life Technologies) with a β-galactosidase vector as a normalization control. The mammalian two-hybrid assays were performed according the published procedures[29]. Transfection mixes included 8 ng $(UAS)_5$-tk-CAT reporter plasmid, 8 ng VP16-human PPARα expression plasmid, 2 ng of either GAL4–N-CoR or GAL4–SMRT expression plasmid, 25 ng β-galactosidase expression plasmid as internal control, and 35 ng carrier plasmid. The synthesis of GW6471 and GW409544 will be described elsewhere.

Binding assays

The effects of GW6471 on the interaction of coactivator and co-repressor peptides with

PPARα were determined by chemical-mediated fluorescence energy transfer assays using the AlphaScreen Technology from Packard BioScience[30]. The experiments were conducted with 5 nM PPARα LBD of biotinylated peptide containing individual motifs (Fig. 3a), following the manufacturer's instructions for the hexahistidine detection kit in a buffer containing 50 mM MOPS, pH 7.4, 50 mM NaF, 0.05 mM CHAPS, 0.1 mg ml^{-1} bovine serum albumin, and 10 mM dithiothreitol (DTT). The binding signals were detected with the increasing concentrations of GW6471, and the results from four repeated experiments were normalized as a percentage of the binding in the absence of GW6471.

The effects of GW6471 on the affinity of the SMRT or N-CoR peptides with purified PPARα LBD were determined by fluorescence polarization in a buffer containing 10 mM HEPES, pH 7.4, 0.15 M NaCl, 3 mM EDTA, 0.005% polysorbate-20, 5 mM DTT and 2.5% DMSO. Varied concentration of PPARα LBD in the presence or absence of 40 μM GW6471 were incubated at room temperature with 10 nM of a fluorescein-labelled peptide of N-CoR2 or SMRT2 (Fig. 3a). The fluorescence polarization values for each concentration of receptor were determined using a BMG PolarStar Galaxy fluorescence reader with 485 nm excitation and 520 nm emission filters. The apparent dissociation constant (K_d) values were determined by the binding curves derived from a nonlinear least-squares-fit of the data for a simple 1:1 interaction.

Mutational analysis of the SMRT co-repressor motif interaction with the PPARα and TRβ LBDs was also performed by fluorescence polarization. To determine the importance of each amino acid in the SMRT motif for binding to nuclear receptors, SMRT peptides with alanine substitution at each position were added to inhibit the binding of 1 μM TRβ LBD or 2 μM PPARα to the fluorescent N-CoR2 peptide. For the PPARα experiments we added 10 μM GW6471. The inhibition curves were constructed and IC_{50} values were determined by nonlinear least-squares-fit of the data to a simple 1:1 interaction.

Received 8 November; accepted 12 December 2001.

1. Horlein, A. J. *et al.* Ligand-independent repression by the thyroid hormone receptor mediated by a nuclear receptor co-repressor. *Nature* **377,** 397–404 (1995).
2. Chen, J. D. & Evans, R. M. A transcriptional co-repressor that interacts with nuclear hormone receptors. *Nature* **377,** 454–457 (1995).
3. Nagy, L. *et al.* Nuclear receptor repression mediated by a complex containing SMRT, mSin3A, and histone deacetylase. *Cell* **89,** 373–380 (1997).
4. Hassig, C. A., Fleischer, T. C., Billin, A. N., Schreiber, S. L. & Ayer, D. E. Histone deacetylase activity is required for full transcriptional repression by mSin3A. *Cell* **89,** 341–347 (1997).
5. Laherty, C. D. *et al.* Histone deacetylases associated with the mSin3 corepressor mediate mad transcriptional repression. *Cell* **89,** 349–356 (1997).
6. Hong, S. H., David, G., Wong, C. W., Dejean, A. & Privalsky, M. L. SMRT corepressor interacts with PLZF and with the PML-retinoic acid receptor alpha (RARα) and PLZF-RARα oncoproteins associated with acute promyelocytic leukemia. *Proc. Natl Acad. Sci. USA* **94,** 9028–9033 (1997).
7. Grignani, F. *et al.* Fusion proteins of the retinoic acid receptor-α recruit histone deacetylase in promyelocytic leukaemia. *Nature* **391,** 815–881 (1998).
8. Yoh, S. M., Chatterjee, V. K. & Privalsky, M. L. Thyroid hormone resistance syndrome manifests as an aberrant interaction between mutant T3 receptors and transcriptional corepressors. *Mol. Endocrinol.* **11,** 470–480 (1997).
9. Jackson, T. A. *et al.* The partial agonist activity of antagonist-occupied steroid receptors is controlled by a novel hinge domain-binding coactivator L7/SPA and the corepressors N-CoR or SMRT. *Mol. Endocrinol.* **11,** 693–705 (1997).
10. Issemann, I. & Green, S. Activation of a member of the steroid hormone receptor superfamily by peroxisome proliferators. *Nature* **347,** 645–650 (1990).
11. Xu, H. E. *et al.* Structural determinants of ligand binding selectivity between the peroxisome proliferator-activated receptors. *Proc. Natl Acad. Sci. USA* **98,** 13919–13924 (2001).
12. Onate, S. A., Tsai, S. Y., Tsai, M. J. & O'Malley, B. W. Sequence and characterization of a coactivator for the steroid hormone receptor superfamily. *Science* **270,** 1354–1357 (1995).
13. Shiau, A. K. *et al.* The structural basis of estrogen receptor/coactivator recognition and the antagonism of this interaction by tamoxifen. *Cell* **95,** 927–937 (1998).
14. Darimont, B. D. *et al.* Structure and specificity of nuclear receptor–coactivator interactions. *Genes Dev.* **12,** 3343–3356 (1998).
15. Gampe, R. T.Jr *et al.* Asymmetry in the PPARγ/RXRα crystal structure reveals the molecular basis of heterodimerization among nuclear receptors. *Mol. Cell* **5,** 545–555 (2000).
16. Nolte, R. T. *et al.* Ligand binding and co-activator assembly of the peroxisome proliferator-activated receptor-γ. *Nature* **395,** 137–143 (1998).
17. Heery, D. M., Kalkhoven, E., Hoare, S. & Parker, M. G. A signature motif in transcriptional co-activators mediates binding to nuclear receptors. *Nature* **387,** 733–736 (1997).
18. Yang, W., Rachez, C. & Freedman, L. P. Discrete roles for peroxisome proliferator-activated receptor gamma and retinoid X receptor in recruiting nuclear receptor coactivators. *Mol. Cell Biol.* **20,** 8008–8017 (2000).
19. Nagy, L. *et al.* Mechanism of corepressor binding and release from nuclear hormone receptors. *Genes Dev.* **13,** 3209–3216 (1999).
20. Hu, X. & Lazar, M. A. The CoRNR motif controls the recruitment of corepressors by nuclear hormone receptors. *Nature* **402,** 93–96 (1999).
21. Perissi, V. *et al.* Molecular determinants of nuclear receptor–corepressor interaction. *Genes Dev.* **13,** 3198–3208 (1999).
22. Zhou, G. *et al.* Nuclear receptors have distinct affinities for coactivators: characterization by fluorescence resonance energy transfer. *Mol. Endocrinol.* **12,** 1594–1604 (1998).
23. Xu, H. E. *et al.* Molecular recognition of fatty acids by peroxisome proliferator-activated receptors. *Mol. Cell* **3,** 397–403 (1999).
24. Otwinowski, Z. & Minor, W. in *Macromolecular Crystallography* (eds Carter, J. C. W. & Sweet, R. M.) 307–326 (Academic, New York, 1997).
25. Navaza, J., Gover, S. & Wolf, W. in *Molecular Replacement: Proceedings of the CCP4 Study Weekend* (ed. Dodson, E. J.) 87–90 (SERC, Daresbury, 1992).
26. Cowtan, K. in *Joint CCP4 and ESF-EACBM Newsletter on Protein Crystallography* **31,** 34–38 (1994).
27. Nolte, R. T., Conlin, R. M., Harrison, S. C. & Brown, R. S. Differing roles for zinc fingers in DNA recognition: structure of a six-finger transcription factor IIIA complex. *Proc. Natl Acad. Sci. USA* **95,** 2938–2943 (1998).
28. Brunger, A. T. *et al.* Crystallography & NMR system: A new software suite for macromolecular structure determination. *Acta Crystallogr. D* **54,** 905–921 (1998).
29. Oberfield, J. L. *et al.* A peroxisome proliferator-activated receptor gamma ligand inhibits adipocyte differentiation. *Proc. Natl Acad. Sci. USA* **96,** 6102–6106 (1999).
30. Ullman, E. F. *et al.* Luminescent oxygen channeling immunoassay: measurement of particle binding kinetics by chemiluminescence. *Proc. Natl Acad. Sci. USA* **91,** 5426–5430 (1994).

Acknowledgements

We thank B. Wisely and R. Bledsoe for making co-repressor expression constructs in early crystallization studies; W. Burkart and M. Moyer for protein sequencing; M. Iannone for compound characterizations; G. Waitt and C. Wagner for mass spectroscopy and amino-acid content analysis; and J. Chrzas and A. Howard for assistance with data collections at 17-ID. Use of the Advanced Photon Source was supported by the US Department of Energy, Basic Energy Sciences, and Office of Science. We also thank L. Kuyper and D. Eggleston for support and critical reading of the manuscript.

Competing interests statement

The authors declare that they have no competing financial interests.

Correspondence and requests for materials should be addressed to H.E.X. (e-mail: ex11957@gsk.com). The Protein Data Bank code for the PPARα/GW6471/SMRT complex and the PPARα/GW409544/SRC-1 complex is 1KQQ and 1K7L, respectively.

correction

Autonomic healing of polymer composites

S. R. White, N. R. Sottos, P. H. Geubelle, J. S. Moore, M. R. Kessler, S. R. Sriram, E. N. Brown & S. Viswanathan

Nature **409,** 794–797 (2001).

In this Letter, the middle infrared spectrum in Fig. 3b, corresponding to an authentic sample of poly(DCPD) prepared with Grubbs' catalyst and DCPD monomer, was a duplicate of the top spectrum owing to a formatting error. The corrected spectra are shown below. □